# Binary Phosphorus–Carbon Compounds: The Series $P_4C_{3+8n}$

FREDERIK CLAEYSSENS, JOSEP M. OLIVA, PAUL W. MAY, NEIL L. ALLAN

*School of Chemistry, University of Bristol, Cantock's Close, Bristol BS8 1TS, UK*

**ABSTRACT:** The structure and stability of periodic solid phosphorus carbide phases $P_4C_{3+8n}$ ($n = 0$–4) are studied at zero and high pressure using periodic density functional theory as implemented in the codes SIESTA and CASTEP. For each composition a range of structures is examined, including both defective diamond-like and graphitic-like structures. At zero pressure the lowest energy structure for $P_4C_3$ ($n = 0$) is defect zinc blende, whereas for compositions richer in carbon ($n > 0$) defect graphitic phases in which some carbon atom are bonded to three phosphorus neighbors are the most stable. We relate the relative stability of the different structures to the bonding and compare the corresponding nitrogen analogues.    © 2003 Wiley Periodicals, Inc. Int J Quantum Chem 95: 546–553, 2003

**Key words:** binary compounds; carbon; density functional theory; phosphorus; carbon phosphide

## Introduction

In recent years a great deal of interest has been shown in developing experimental methods to produce binary nitrides that are isoelectronic with diamond, and in particular carbon nitride ($C_3N_4$). This follows theoretical predictions that $C_3N_4$ should have a bulk modulus in excess of that of diamond [1]. Additionally, the size of the predicted band gap (~3.5 eV) would make it potentially attractive for optical and electronic applications such as light-emitting diodes (LEDs) or diode lasers. Unfortunately preparation of crystalline carbon nitride has proved to be extremely laborious, and to date only small amounts of crystalline material have been synthesized, only in the form of thin films of a few micrometers' thickness. Most of the physical processes used for carbon nitride deposition, such as laser ablation [2], cathodic arc deposition [3] and chemical vapor deposition [4] yield amorphous films with a low percentage of nitrogen in the films (1–10%).

In sharp contrast to the experimental impasse in producing carbon nitride crystallites with a high nitrogen content, phosphorus carbide has been produced as amorphous thin films over a wide range of P:C compositions (up to a ratio of 3:1) ratios via

**TABLE I** _____

Calculated lattice parameters (Å), symmetries and energies (eV/formula unit) for the four $P_4C_3$ structures lowest in energy from SIESTA and CASTEP calculations.

| Space group | P$\bar{4}$3m (215) | P63mc (186) | P112 (3) | P$\bar{6}$m2 (187) |
|---|---|---|---|---|
| CASTEP |  |  |  |  |
| Volume (Å$^3$) | 70.45 | 71.37 | 92.77 | 102.14 |
| Energy (eV/formula unit) | −1189.41 | −1189.18 | −1188.68 | −1188.24 |
| a | 4.130 | 5.803 | 4.038 | 5.765 |
| b | 4.130 | 5.803 | 5.705 | 5.765 |
| c | 4.130 | 4.872 | 5.136 | 7.111 |
| γ |  |  | 130.5° |  |
| SIESTA |  |  |  |  |
| Volume (Å$^3$) | 76.30 | 76.95 | 96.76 | 104.08 |
| Energy (eV/formula unit) | −1177.43 | −1177.09 | −1176.24 | −1175.57 |
| a | 4.241 | 5.959 | 4.069 | 5.930 |
| b | 4.241 | 5.959 | 5.890 | 5.930 |
| c | 4.241 | 5.005 | 5.259 | 6.834 |
| γ |  |  | 129.9° |  |

capacitively coupled radio frequency (RF) plasma deposition from $PH_3/CH_4$ gas mixtures [5]. Because of the very high P content, these films cannot realistically be called doped diamond-like carbon (DLC) films. Since recent investigations strongly suggest that the deposited films do exist as an amorphous network, as opposed to segregated carbon and phosphorus phases, they can legitimately be called amorphous phosphorus carbide films.

These experimental results together with the substantial volume of theoretical work on carbon nitrides (see, e.g., Refs. 1, 6–8) have led us to start a complementary computational study of possible stable forms of solid phosphorus carbide phases $P_xC_y$. Our preliminary results [9] for $P_4C_3$ suggest a favoring of diamond-like structures over graphitic, unlike $C_3N_4$. In the current article we extend these studies and examine the series $P_4C_{3+8n}$ ($n = 0, 1, 2, 3, 4$) and thus a wide range of P:C ratios using periodic ab initio density functional calculations. Electron-counting rules indicate that in this series P—P bonds in the formula unit are not required in order to have a filled valence band and nonmetallic behavior. The only $P_xC_y$ stoichiometry requiring neither C—C nor P—P bonds in the formula unit is $P_4C_3$. We relate the relative stability of the different structures to the local environment of the C and P atoms and compare the molecular chemistry of these elements.

## Computational Details

Calculations were carried out using: periodic numerical atomic orbitals density functional theory (DFT) in the generalized gradient approximation (GGA) as implemented in the SIESTA code [10], with the exchange-correlation functional of Perdew, Burke, and Ernzerhof [11]; and GGA plane-wave DFT calculations with the Perdew–Wang exchange correlation functional [12].
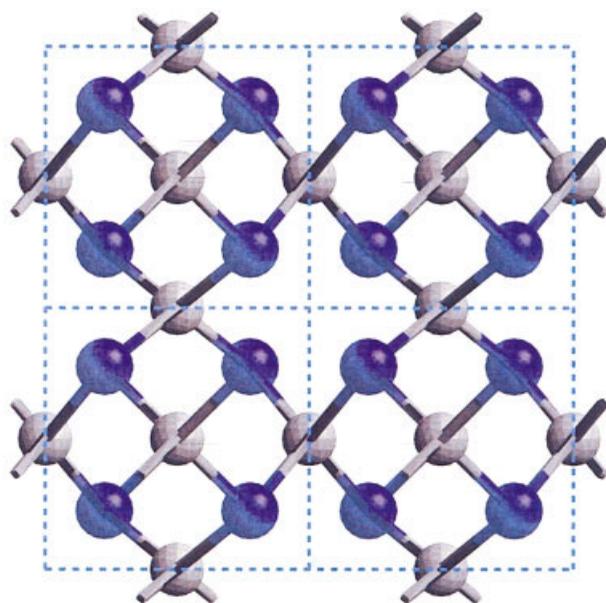
Only the valence electrons are considered in both sets of calculations. In the SIESTA calculations, core electrons are replaced by norm-conserving scalar pseudopotentials [13] factorized in the Kleinman–Bylander form [14]. The pseudopotentials for carbon and phosphorus were generated with the following atomic configurations and cutoff radii for s, p, d, and f components, respectively: C → [He]$2s^2 2p^2$, 1.25 a.u. for all components; P → [Ne]$3s^2 3p^3$, 1.85 a.u. for all components. A split-valence double-$\zeta$ basis set is used including a set of polarization 3d functions on both C and P atoms, as obtained with an energy shift of 250 meV. To obtain the Hamiltonian matrix elements, the electron integrals of the self-consistent terms are computed with the help of a regular space grid onto which the electron density is projected. The grid spacing is determined by the maximum kinetic energy of the plane waves that can be represented in that grid. In our calculations, the cutoff is 225 Ry. The cell parameters and atomic positions were relaxed and

optimized by energy minimization using a conjugate-gradient algorithm with a maximum force tolerance 0.02 eV $\text{Å}^{-1}$ and a maximum stress component of 0.5 GPa. In the CASTEP calculations we used the ultrasoft Vanderbilt potentials [15] and an energy cutoff for the plane waves of at least 310 eV. With both codes, we checked that all results were well converged with respect to the real space grid, Brillouin zone sampling, basis set, and geometry relaxation parameters.
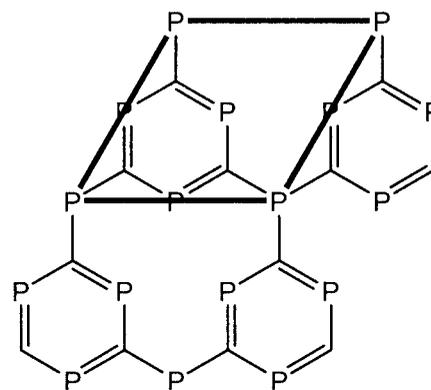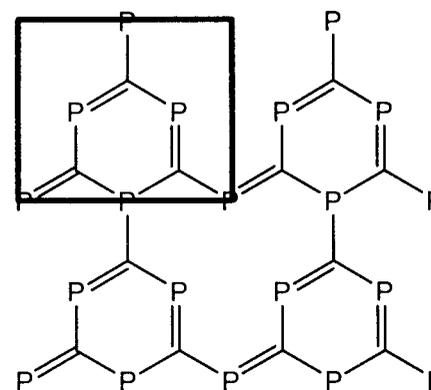
## Results

### STRUCTURES

We start with $P_4C_3$ and seven candidate structures. These include the five possibilities suggested for $C_3N_4$ by Teter and Hemley [1]: $\alpha$-, $\beta$- ($\beta$-$Si_3N_4$), and cubic (high-pressure willemite-II $Zn_2SiO_4$), and pseudocubic ($\alpha$-$CdIn_2Se_4$) forms together with one hexagonally-closed-packed graphitic structure. The other two are a defect wurtzite structure and a further graphitic phase with the alternative vacancy ordering suggested by Mattesini et al. [16]. Table I lists the resulting lattice parameters and energies of the four structures lowest in energy. The pseudocubic form [space group $P\bar{4}3m$ (215)] shown in Figure 1 and based on a defect zinc-blende structure is the



**FIGURE 1.** Crystal structure of the pseudocubic phase of $P_4C_3$. Dark grey and blue spheres denote carbon and phosphorus atoms, respectively. Dashed black line denotes the unit cell.
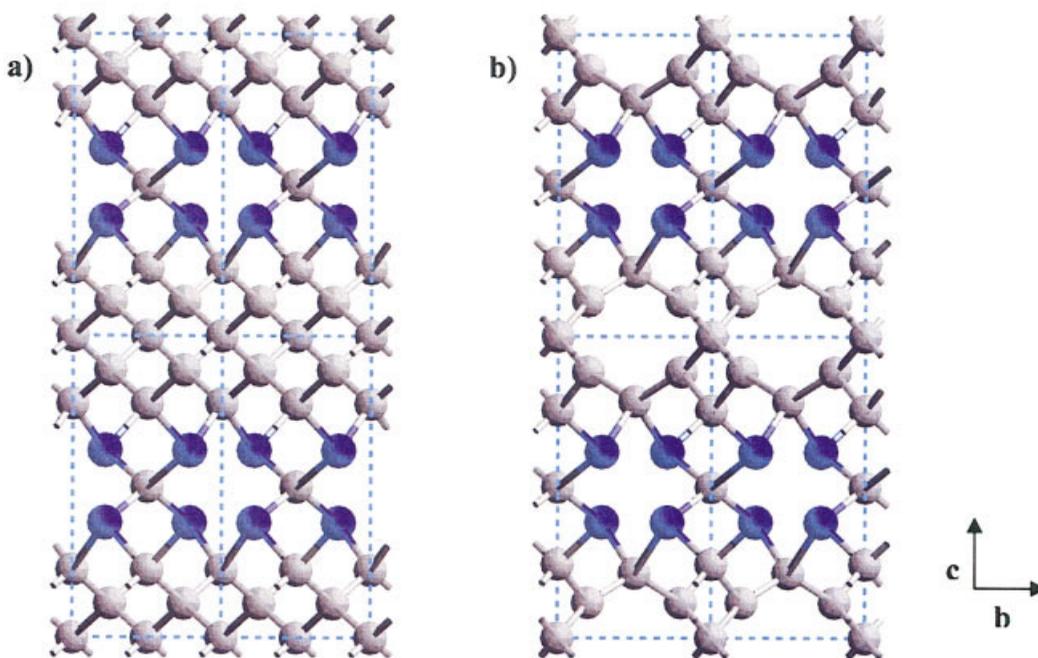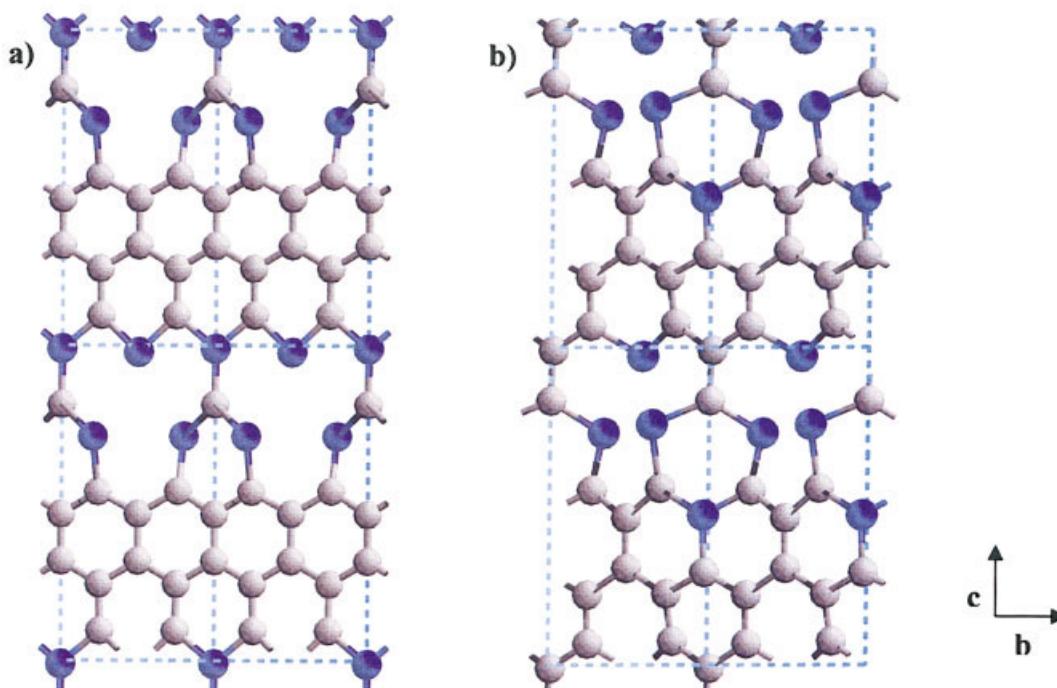


**FIGURE 2.** Possible vacancy orderings for graphitic $P_4C_3$. (a) Hexagonal unit cell. (b) Orthorhombic unit cell.

lowest in energy. Thus, structures low in energy for $C_3N_4$ are high in energy for $P_4C_3$. The CPC bond angles in the high-energy $\alpha$, $\beta$, and cubic phases (not listed in Table I) are all considerably larger (typically 110–115°) than those in the pseudocubic phase ($\approx$104°), which are closer to the CPC bond angle in the molecule $P(CH_3)_3$ (99°). A second low-energy structure is a hexagonal-defect wurtzite structure [$P63mc$ (186)], which is only $\approx$0.3 eV/(formula unit) higher in energy than the pseudocubic. As in the pseudocubic structure, the CPC bond angles are $\approx$104°. This is consistent with the known molecular chemistries of N and P, where P shows a much more marked preference than N for pyramidal coordination. The preference for the zinc-blende over the wurtzite form is also in keeping with a favoring of six-membered rings in chair rather than boat conformations.

Turning to graphitic forms of $P_4C_3$, we considered two vacancy orderings, as shown in Figure 2. The unit cell of the first, proposed by Teter and Hemley [1], is hexagonal and is related to the

**FIGURE 3.** Crystal structures of possible $P_4C_{11}$ analogues of pseudocubic $P_4C_3$: (a) low-energy tetragonal form; and (b) high-energy orthorhombic structure. Dark grey and blue spheres denote carbon and phosphorus atoms, respectively. Dashed black line denotes the unit cell.



**FIGURE 4.** Crystal structures of the $P_4C_{11}$ analogues of the graphitic $P_4C_3$: (a) ordering (A); (b) ordering (B), in which no carbon atom is bonded to more than two phosphorus atoms. Dark grey and blue spheres denote carbon and phosphorus atoms, respectively.

**TABLE II**

Calculated lattice parameters (Å), symmetries and energies (eV/formula unit) for the four $P_4C_{11}$ structures lowest in energy.[a]

| Structure | Tetragonal pseudocubic | Orthorhombic pseudocubic | Graphitic (A) | Graphitic (B) |
|---|---|---|---|---|
| **CASTEP** | | | | |
| Space group | $P\bar{4}2m$ (111) | $P222$ (16) | $P2$ (3) | $P1$ (1) |
| Volume (Å³/formula unit) | 110.30 | 119.75 | 167.59 | 172.48 |
| Energy (eV/formula unit) | −2433.74 | −2422.86 | −2435.36 | −2435.12 |
| $a$ | 3.78 | 3.94 | 3.82 | 4.18 |
| $b$ | 3.78 | 3.90 | 5.08 | 5.15 |
| $c$ | 7.72 | 7.80 | 9.53 | 9.14 |
| $\alpha$ | | | | 92.1° |
| $\beta$ | | | | 86.9° |
| $\gamma$ | | | 115.1° | 118.5° |
| **SIESTA** | | | | |
| Space group | $P\bar{4}2m$ (111) | $P222$ (16) | $P2$ (3) | $P1$ (1) |
| Volume (Å³/formula unit) | 117.83 | 128.10 | 173.48 | 171.86 |
| Energy (eV/formula unit) | −2412.15 | −2400.90 | −2412.52 | −2412.43 |
| $a$ | 3.86 | 4.02 | 4.34 | 4.28 |
| $b$ | 3.86 | 3.94 | 5.22 | 5.24 |
| $c$ | 7.92 | 8.10 | 9.65 | 9.26 |
| $\alpha$ | | | | 90.4° |
| $\beta$ | | | | 85.1° |
| $\gamma$ | | | 127.5° | 123.7° |

[a] Tetragonal and orthorhombic pseudocubic refer to the structures shown in Figures 3a and 3b, respectively. Graphitic (A) and graphitic (B) refer to the two orderings shown in Figures 4a and 4b, respectively.

pseudocubic form considered earlier by a rhombohedral distortion. The space group is $P\bar{6}m2$ (187) (AB stacking of graphitic layers). The second is the orthorhombic form [initial space group $P2mm$ (25)], proposed in Ref. 16. This second ordering, unlike the first, is associated with a formal delocalization of the $\pi$-electrons over the graphite-like planes. Graphitic forms for $P_4C_3$ are higher in energy than are diamond-like forms, unlike for $C_3N_4$, where these lie lowest in energy [1]. This is in line with the well-known preference of P and other second-row elements for single, rather than multiple, bond formation in molecules. In addition, we observe a greater tendency for the graphitic $P_4C_3$ networks to buckle to allow a pyramidal rather than planar coordination of the phosphorus atoms. Graphitic C—P bond lengths (typically $\approx$1.79 Å in the SIESTA calculations, 1.76 Å from CASTEP) are shorter than the single C—P bonds in the pseudocubic phase, as expected (typically $\approx$1.91 Å and 1.86 Å from the SIESTA and CASTEP calculations, respectively). The layers in the orthorhombic form show considerably more distortion from the ideal flat graphitic structure than do those in the hexagonal, with a short interplanar P—P distance. After optimization, the final space group is $P112$ (3), and of the two graphitic forms investigated this is the lower in energy.

Turning to $P_4C_{11}$, a "pseudocubic" $P_4C_{11}$ structure is readily generated from that for pseudocubic $P_4C_3$ by doubling the unit cell along one lattice vector, adding one carbon atom at the center of the second cell, and replacing the new four phosphorus atom with carbon atoms. An alternative way of viewing this structure is to view the unit cell of $P_4C_{11}$ as comprising a cubic unit cell of diamond ($C_8$) adjacent to a pseudocubic unit cell of $P_4C_3$. The resulting tetragonal structure is shown in Figure 3a, whereas a different choice of phosphorus substitution gives rise to the orthorhombic structure in Figure 3b. Two possible choices for graphitic $P_4C_{11}$, which we denote as graphite(A) and graphite(B), respectively, are given in Figures 4a and 4b. These differ in the number of P atoms directly bonded to C. In graphite(A) some carbons are bonded to three P atoms, whereas in graphite(B) carbon atoms have no more than two nearest phosphorus neighbors. The layers are stacked $AB$ in each case, with a monoclinic unit cell ($\gamma \neq 90°$). Both (A) and (B)

**TABLE III**

Calculated lattice parameters (Å) and energies (eV/formula unit) for the tetragonal pseudocubic (pc) and graphitic (A) (gr) structures of $P_4C_{19}$, $P_4C_{27}$ and $P_4C_{35}$.

| Structure | $P_4C_{19}$ pc | $P_4C_{19}$ gr | $P_4C_{27}$ pc | $P_4C_{27}$ gr | $P_4C_{35}$ pc | $P_4C_{35}$ gr |
|---|---|---|---|---|---|---|
| CASTEP | | | | | | |
| Volume (Å³/formula unit) | 153.54 | 248.17 | 197.72 | 336.90 | 241.51 | 424.91 |
| Energy (eV/formula unit) | −3680.96 | −3684.56 | −4928.78 | −4935.36 | −6176.71 | −6184.78 |
| $a$ | 3.69 | 4.14 | 3.65 | 4.48 | 3.63 | 4.61 |
| $b$ | 3.69 | 4.99 | 3.65 | 4.91 | 3.63 | 4.91 |
| $c$ | 11.27 | 13.68 | 14.83 | 17.78 | 18.35 | 21.99 |
| $\alpha$ | | 90.0° | | 89.8° | | 90.0° |
| $\beta$ | | 90.0° | | 92.7° | | 92.4° |
| $\gamma$ | | 118.7° | | 120.7° | | 121.2° |
| SIESTA | | | | | | |
| Volume (Å³/formula unit) | 163.00 | 246.46 | 208.41 | 319.90 | | |
| Energy (eV/formula unit) | −3649.57 | −3652.44 | −4887.78 | −4891.40 | | |
| $a$ | 3.75 | 4.42 | 3.71 | 4.45 | | |
| $b$ | 3.75 | 5.04 | 3.71 | 5.02 | | |
| $c$ | 11.58 | 13.86 | 15.17 | 18.08 | | |
| $\alpha$ | | 90.2° | | 89.9° | | |
| $\beta$ | | 95.4° | | 83.3° | | |
| $\gamma$ | | 126.6° | | 126.8° | | |

vacancy orderings are more similar to the second vacancy ordering for $P_4C_3$ in Figure 2 than to the first, because all three P atoms closest to the carbon vacancy are two- rather than three-coordinate.

Table II lists the optimized energies and lattice parameters for these four structures, which are also those considered for $C_{11}N_4$ by Mattesini and Matar [8]. It is striking that, unlike $P_4C_3$, the graphitic structures (A) and (B) now lie lower in energy than do the diamond-like forms. Of the two graphitic structures (A) is lower in energy than is (B) (as noted also [8] for $C_{11}N_4$) by 0.1 eV per formula unit (SIESTA) and 0.2 eV per formula unit (CASTEP). Of the four structures we have considered, the highest in energy (by >10 eV) is the orthorhombic pseudocubic structure, which is not unexpected, because this contains several carbon atoms with "dangling" bonds adjacent to a carbon vacancy. The energy ordering of the four structures is identical to that for $C_{11}N_4$ [8].

Presumably, the enhanced stability of the graphitic structure compared with $P_4C_3$ is ultimately due to the larger carbon content. The C—P bonds are appreciably weaker than are the C—C bonds [17], and the graphitic forms have an appreciably higher ratio of C—C:C—P bonds than do the pseudocubic. There is also an appreciable mismatch between the lattice parameters of diamond (3.57 Å CASTEP) and that of pseudocubic $P_4C_3$ (4.13 Å CASTEP). The "ideal"

C—C bond length (1.54 Å) and the CCC angle (109.5°) observed in the diamond structure are distorted in the tetragonal pseudocubic $P_4C_{11}$ structure [$P\bar{4}2m$ (111)] to 1.58–1.61 Å and 106.6–114.4°, respectively (from CASTEP; SIESTA results are very similar). The C—P bond lengths and CPC bond angles are also different in $P_4C_{11}$ from those in $P_4C_3$; the C—P bond is shorter, on average, by 0.08 Å and instead of just one value in $P_4C_3$ (104°), there is a considerable variation in the CPC angles from 95.5° to 105.3°. All of these structural parameters indicate a mismatch-induced stress in $P_4C_{11}$. The calculated lattice parameters for the tetragonal pseudocubic $P_4C_{11}$ indicate that $a$ and $b$ are smaller than the average value (3.85 Å) anticipated from Vegard's Law and the lattice parameters of diamond and $P_4C_3$. This deviation from a linear interpolation is consistent with the higher-bulk modulus of diamond relative to that of $P_4C_3$.

The mismatch is less important for the lower-dimensional graphitic structures. The layers in these structures show considerable distortion from the ideal flat graphitic structure, with some short interlayer P—P distances. Overall, graphitic C—P bonds are similar to those in the graphitic form of $P_4C_3$ and C—C bonds close to those in graphite itself. Variations in the CPC angles leading to a pronounced out-of-plane distortion and buckling of the layers, indicating once more the preference of phosphorus for nonplanar geometries.
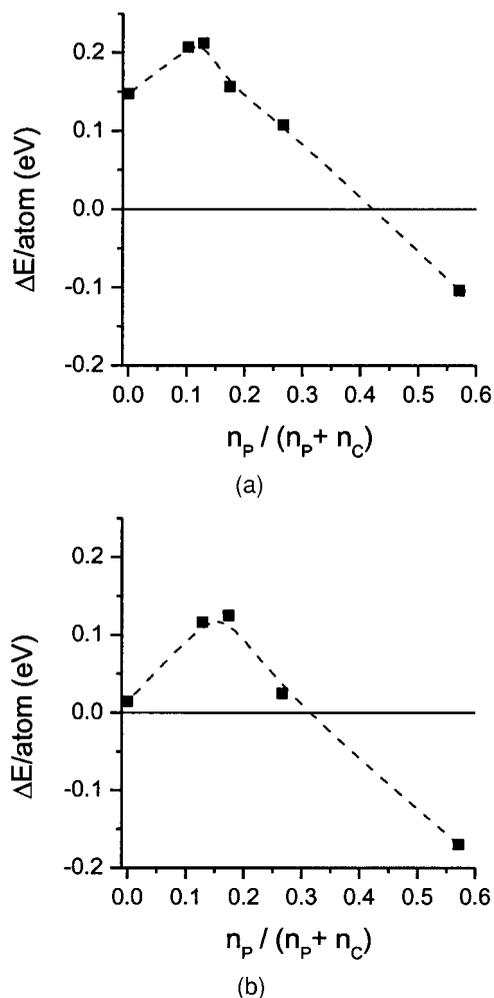
We also carried out calculations for $P_4C_{19}$, $P_4C_{27}$, and $P_4C_{35}$. Each successive structure was generated from the preceding one in the same way that of $P_4C_{11}$ was produced from $P_4C_3$. Only the analogues of the lowest pseudocubic and graphitic energy structures for $P_4C_{11}$ were considered. For each of these three compounds, the graphitic phase is lower in energy than is the pseudocubic, as anticipated because of the extra carbon content. Optimized lattice parameters and corresponding total energies are listed in Table III.

## Discussion

We next consider the variation of a number of properties with composition. Figure 5 shows the calculated energy difference between the graphitic and diamond forms as a function of phosphorus content. Our CASTEP calculations overestimate the stabilization of the graphitic form of carbon relative to that of diamond (by about 0.2 eV per atom). The difference in energy (0.02 eV per atom) suggested by the SIESTA results is in better agreement with experiment. The stability of layered systems such as graphite where the layers interact only by weak van der Waals interactions is a well-known problem [18] for DFT. Even though the layers in the P-containing graphitic compounds interact more strongly than the layers in graphite, because of the bond polarization $C^{\delta-}$-$P^{\delta+}$, this remains problematic.

Nevertheless, we stress that similar trends across the series $P_4C_{3+8n}$ are observed in both sets of calculations with a crossover in relative stability of graphite and diamond-like forms between $P_4C_3$ and $P_4C_{11}$. The energy difference between diamond and graphite forms is a maximum at phosphorus mole fractions $\approx 0.15$–$0.2$. This variation is a consequence of the larger fraction of C—C to C—P bonds in the graphitic structures, which are stabilized due to the relative strengths of these bonds and of the size mismatch, which destabilizes the pseudocubic structure at large carbon compositions.
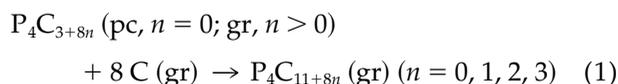
This energy difference is important for the behavior at high pressure. All diamond-like phases are lower in volume than the graphitic, and thus at high pressure the diamond forms become more stable relative to the graphitic. For example, results using SIESTA indicate that in the static limit at 4 GPa the enthalpy ($U + pV$) of the tetragonal pseudocubic form is now lower than that of the graphitic for $P_4C_{11}$ but not for $P_4C_{19}$. We therefore reoptimized the lowest-energy pseudocubic and
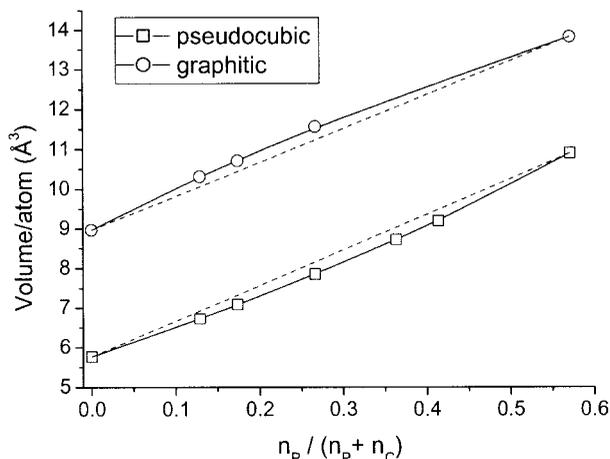


**FIGURE 5.** Variation of the difference in energy between pseudocubic and graphitic-like ($E_{pseudocubic}$ − $E_{graphitic}$) forms with composition, from (a) CASTEP and (b) SIESTA calculations.

graphitic forms for each structure as a function of pressure. Transition pressures of $\approx 3$ GPa, $\approx 6.5$ GPa, and $\approx 6$ GPa are predicted in turn for $P_4C_{11}$, $P_4C_{19}$ and $P_4C_{27}$. For comparison the graphite–diamond transition itself is predicted to be at $\approx 2$ GPa. This nonlinear variation of transition pressure with carbon content is consistent with the energy differences between the graphitic and diamond forms for each composition at zero pressure.

The thermodynamic stability of the series as a function of composition is related to the energy $\Delta E$ of the following reaction:

$$P_4C_{3+8n} \text{ (pc, } n = 0; \text{ gr, } n > 0)$$
$$+ 8\,C\,(gr) \rightarrow P_4C_{11+8n}\,(gr)\,(n = 0, 1, 2, 3) \quad (1)$$

**FIGURE 6.** Volumes of the lowest-energy pseudocubic and graphitic forms as a function of composition from SIESTA. CASTEP results are similar.

For values of $n = 0, 1$, and 2, SIESTA values of $\Delta E$ are 4.3 eV, $-0.9$ eV, and 0.1 eV, respectively. No corrections for zero-point vibration were made. Thus, $P_4C_{19}$ is predicted to be thermodynamically the most stable of $P_4C_{11}$, $P_4C_{19}$, and $P_4C_{27}$; $P_4C_3$ is the most stable of all the systems we studied. We estimate the energy of formation of $P_4C_3$ from black phosphorus and graphite as $\approx 3.2$ eV, and so the formation of all these compounds is endo-energetic. They might still be formed under conditions of kinetic control such as under deposition.

Figure 6 shows the calculated volume per atom as a function of composition for the pseudocubic and graphitic phases. This plot shows clearly a positive deviation from linearity for the pseudocubic phase and a negative deviation for the graphitic phase, in line with the likely different mismatch-induced stresses in the two types of structure.

## Conclusions

In this paper we examined the stability of periodic solid phosphorus carbide phases $P_4C_{3+8n}$ ($n = 0$–4) at zero and high pressure using periodic DFT. At zero pressure, the lowest-energy structure for $P_4C_3$ ($n = 0$) is defect zinc blende, unlike $C_3N_4$. Structures low in energy for $C_3N_4$ are high in energy for $P_4C_3$. In con-

trast, for $P_4C_{11}$ (and higher-carbon compositions), defect graphitic phases in which some carbon atoms are bonded to three phosphorus neighbors are the most stable, similar to that of the corresponding nitrogen analogues. In future work, we will concentrate on the detailed electronic structure of these phases and other stoichiometries.

## References

1. Teter, D. M.; Hemley, R. J. Science 1996, 271, 53.
2. Voevodin, A. A.; Jones, J. G.; Zabinski, J. S.; Czigany, Z.; Hultman, L. J Appl Phys 2002, 92, 4980.
3. Zhou, Z. M.; Xia, L. F. J Phys D Appl Phys 2002, 35, 1991.
4. Popov, C.; Plass, M. F.; Kassing, R.; Kulisch, W. Thin Solid Films 1999, 356, 406.
5. Pearce, S. R. J.; May, P. W.; Wild, R. K.; Hallam, K. R.; Heard, P. J. Diam Relat Mater 2002, 11, 1041.
6. Kim, E.; Chen, C.; Kohler, Y.; Elstner, M.; Frauenheim, T. Phys Rev Lett 2001, 86, 652.
7. Cote, M.; Cohen, M. L. Phys Rev B 1997, 55, 5684.
8. Mattesini, M.; Matar, S. F. Phys Rev B 2002, 65, 075110.
9. Claeyssens, F.; Allan, N. L.; May, P. W.; Ordejón, P.; Oliva, J. M. Chem Commun 2002, 2494.
10. Soler, J. M.; Artacho, E.; Gale, J. D.; García, A.; Junquera, J.; Ordejón, P.; Sánchez-Portal, D. J Phys Condens Mat 2002, 14, 2745.
11. Perdew, J. P.; Burke, K.; Ernzerhof, M. Phys Rev Lett 1996, 77, 3865.
12. Perdew, J. P.; Wang, Y. Phys Rev B 1992, 45, 13244.
13. Trouiller, N.; Martins, J. L. Phys Rev B 1991, 43, 1993.
14. Kleinman, L.; Bylander, D. M. Phys Rev Lett 1982, 48, 1425.
15. Vanderbilt, D. Phys Rev B 1990, 41, 7892.
16. Mattesini, M.; Matar, S. F.; Etourneau, J. J Mater Chem 2000, 10, 709.
17. See, for example, Emsley, J. The Elements, 3rd edition; Clarendon Press: Oxford, 1998.
18. Kim, Y.-H.; Lee, I.-H.; Nagaraja, S.; Leburton, J.-P.; Hood, R. Q.; Martin, R. M. Phys Rev B 2000, 61, 5202.